

InvFussion: Bridging Supervised and Zero-shot Diffusion for Inverse Problems

Noam Elata^{*1} Hyungjin Chung^{*2,3} Jong Chul Ye² Tomer Michaeli¹ Michael Elad¹

¹Technion, Haifa, Israel ²KAIST, Daejeon, South Korea ³EverEx, Seoul, South Korea

{noamelata@campus, tomer.m@ee, elad@cs}.technion.ac.il {hj.chung, jong.ye}@kaist.ac.kr

Abstract

*Diffusion Models have demonstrated remarkable capabilities in handling inverse problems, offering high-quality posterior-sampling-based solutions. Despite significant advances, a fundamental trade-off persists, regarding the way the conditioned synthesis is employed: Training-based methods achieve high quality results, while zero-shot approaches trade this with flexibility. This work introduces a framework that combines the best of both worlds – the strong performance of supervised approaches and the flexibility of zero-shot methods. This is achieved through a novel architectural design that seamlessly integrates the degradation operator directly into the denoiser. In each block, our proposed architecture applies the degradation operator on the network activations and conditions the output using the attention mechanism, enabling adaptation to diverse degradation scenarios while maintaining high performance. Our work demonstrates the versatility of the proposed architecture, operating as a general MMSE estimator, a posterior sampler, or a Neural Posterior Principal Component estimator. This flexibility enables a wide range of downstream tasks, highlighting the broad applicability of our framework. The proposed modification of the denoiser network offers a versatile, accurate, and computationally efficient solution, demonstrating the advantages of dedicated network architectures for complex inverse problems. Experimental results on the FFHQ and ImageNet datasets demonstrate state-of-the-art posterior-sampling performance, surpassing both training-based and zero-shot alternatives.*¹

1. Introduction

Diffusion models [26, 45, 48] have emerged as a leading class of generative machine learning techniques [14, 40]. Since their inception, diffusion models have gained significant traction in solving complex inverse problems, such as

super-resolution [43] or in-painting [35], where the goal is to reconstruct or estimate an underlying image from partial or degraded observations.

Diffusion models can be trained to solve inverse problems using a simple conditioning framework, in which the measurements are supplied to the network [42, 43]. Although powerful, these methods are typically restricted to handling a limited set of degradations per trained network. This is because during training, the network must infer the connection between clean images and their degraded versions, even when a closed-form relation for each possible degradation is known. And at test time, the network must infer from the input which among the possible degradation processes generated it (a blind restoration setting). This fundamental limitation significantly reduces the applicability of trained conditional diffusion-based methods, as in many cases it is required to accommodate a wide range of inverse problems. Conversely, zero-shot methods [8, 9, 30, 31, 47] utilize unconditional pre-trained diffusion models for solving inverse problems, taking into account the particular degradation process from which each input suffers (a nonblind setting). They are thus remarkably flexible in handling various degradation scenarios. However, these approximate approaches suffer from reduced accuracy and computational inefficiency.

Here, we introduce an architectural framework that combines the strengths of the training-based and zero-shot methodologies. Our approach relies on a new network architecture that is conditioned on the degradation operator. This conditioning enables the network to make full use of the provided measurements. Since the set of all possible degradations is too large to be used directly as a model input, we propose integrating the degradation operator into the architecture’s design, implicitly enabling the network to infer whether its intermediate features are consistent with the measurements. This novel architecture allows the network to adapt to virtually any degradation, while simultaneously maintaining the high-performance of training-based networks. Our method represents a paradigm shift, offering a more versatile, accurate, and computationally efficient ap-

^{*}Equal Contribution.

¹Code at <https://github.com/noamelata/InvFussion>.



Figure 1. **Examples for posterior samples from our degradation-aware diffusion model at 256×256 resolution.** A single model can restore multiple degradations, such as in-painting, de-blurring and super-resolution with high image fidelity and realism, by integrating the degradation operator into the model’s architecture.

proach to handling complex inverse problems.

Our network’s architecture is inspired by unrolling frameworks [1, 50, 57], in which the layers mimic an optimization process. In our case, we integrate the degradation operator within the network’s layers using attention mechanisms [15, 39, 53]. The attention layers preserve dimensionality, and thus enable applying the degradation operator to all network activations. We use HDiT [11] as our base architecture, which is particularly effective in facilitating operations on higher-resolution images, as shown in Fig. 1.

Accordingly, while traditional training-based methods cannot handle scenarios where it is impossible to infer the degradation process from the measurements, and zero-shot methods are inaccurate, our model offers significant advantages in both computational efficiency and flexibility. In particular, our method can be used with any sampler for unconditional diffusion models [28, 33, 34], including Classifier-Free Guidance (CFG) [10, 25] and related techniques. Beyond posterior sampling, we illustrate how our architecture can be used for outputting the Minimum Mean Square Error (MMSE) predictor, as well as for training a Neural Posterior Principal Component (NPPC) [38] predictor, enabling uncertainly quantification for a wide variety of restoration tasks with one model.

Our experimental results on FFHQ [27] and ImageNet [13] demonstrate superior performance compared to existing inverse problem solvers, both training-based and zero-shot, establishing a new state-of-the-art (SOTA).

2. Background and Related Work

2.1. Diffusion Models

Diffusion Models [26, 45, 48] generate high-quality images through a sequential Gaussian noise removal process. Given a source data distribution $p(\mathbf{x}_0)$, a forward diffu-

sion process constructs a Stochastic Differential Equation (SDE) $d\mathbf{x}_t = -\frac{1}{2}\beta(t)\mathbf{x}_t + \sqrt{\beta(t)}d\mathbf{w}_t$, where \mathbf{w}_t is a standard Wiener process and $\beta(t)$ is a deterministic function of $t \in [0, 1]$ taken such that at $t = 1$, the final marginal distribution $p(\mathbf{x}_1)$ becomes approximately a standard Gaussian. Each marginal distribution along this SDE, $p(\mathbf{x}_t)$, can be constructed directly by adding Gaussian noise to the source data distribution, $\mathbf{x}_t = \sqrt{\bar{\alpha}(t)}\mathbf{x}_0 + \sqrt{1 - \bar{\alpha}(t)}\epsilon$, where $\bar{\alpha}(t) = e^{-\int_0^t \beta(s)ds}$ and ϵ is a standard Gaussian random vector. To generate a sample image within this framework, one starts with a sample of white Gaussian noise and employs an appropriate SDE solver [28, 33, 34] for the reverse SDE [3, 37, 49]. The latter requires knowing the score $\nabla_{\mathbf{x}_t} \log(p(\mathbf{x}_t))$ [46, 48, 49]. By exploiting the connection between the score and the MMSE predictor [2, 54], $\mathbf{x}_t + (1 - \bar{\alpha}(t))\nabla_{\mathbf{x}_t} \log(p(\mathbf{x}_t)) = \sqrt{\bar{\alpha}(t)}\mathbb{E}[\mathbf{x}_0|\mathbf{x}_t]$, a denoising network trained to approximate $\mathbb{E}[\mathbf{x}_0|\mathbf{x}_t]$ can be used in place of the real score function. Training such a network is done using a regression loss,

$$\mathcal{L} = \mathbb{E} \left[w_t \|m_\theta(\mathbf{x}_t, t) - \mathbf{x}_0\|^2 \right], \quad (1)$$

where m_θ is the model being trained, $\mathbf{x}_0 \sim p(\mathbf{x}_0)$, and w_t is some weighting function.

2.2. Inverse Problems

Inverse problem solvers attempt to reverse a degradation process that corrupted an image $\mathbf{x} \in \mathbb{R}^D$ and yielded measurements $\mathbf{y} \in \mathbb{R}^d$. Many common degradations, such as those encountered in the super-resolution, deblurring, denoising, and in-painting tasks, have a linear form. These degradations are often written as $\mathbf{y} = \mathbf{H}\mathbf{x} + \mathbf{n}$ where $\mathbf{H} \in \mathbb{R}^{d \times D}$ and $\mathbf{n} \sim \mathcal{N}(0, \sigma_n^2 \mathbf{I})$ is white Gaussian noise added to the measurements. Noiseless measurements can be formulated with $\sigma_n = 0$. When attempting to design

a system that can handle multiple degradations, \mathbf{H} can be considered a random matrix drawn from some distribution of possible corruption operators.

A popular approach for generating a reconstruction $\hat{\mathbf{x}}$ of \mathbf{x} based on the measurement \mathbf{y} and on knowledge of \mathbf{H} , is to draw $\hat{\mathbf{x}}$ from the posterior distribution,

$$\hat{\mathbf{x}}_{\text{Post}} \sim p(\mathbf{x}|\mathbf{y}, \mathbf{H}). \quad (2)$$

Methods aiming for this solution are called posterior samplers and are the main focus of this work. Another popular approach to generating a reconstruction, is by aiming for the Minimum Mean Square Error (MMSE) predictor,

$$\hat{\mathbf{x}}_{\text{MMSE}} = \mathbb{E}[\mathbf{x}|\mathbf{y}, \mathbf{H}], \quad (3)$$

which, as its name implies, achieves the lowest possible squared-error distortion. Obtaining an approximation of the MMSE predictor can be done by training a regression network $m_\theta(\mathbf{y})$ to minimize $\mathcal{L} = \mathbb{E}[\|m_\theta(\mathbf{y}) - \mathbf{x}\|^2]$.

When the degradation operator \mathbf{H} is not known, or is known but cannot be provided to the model, the relevant posterior distribution is

$$p(\mathbf{x}|\mathbf{y}) = \int p(\mathbf{x}|\mathbf{y}, \mathbf{H})p(\mathbf{H}|\mathbf{y})d\mathbf{H}. \quad (4)$$

This posterior is a weighted average of all possible posterior distributions (for all possible degradations \mathbf{H}), each weighted by the corresponding $p(\mathbf{H}|\mathbf{y})$. This posterior may generally encompass a significantly larger uncertainty regarding \mathbf{x} . One key limitation of training-based posterior samplers is that they lack a mechanism to condition the model on \mathbf{H} . Therefore, even if \mathbf{H} is known, it cannot be provided to the model at test time, so that the model is unavoidably tasked with solving a blind restoration problem. Here, we introduce a *degradation-aware* model architecture, which allows solving the easier nonblind restoration task whenever the degradation is known at test time.

2.3. Diffusion Restoration

In recent years, diffusion models have become the leading approach for posterior sampling. By modifying the probability distribution into a conditional one, $p(\mathbf{x}_t|\mathbf{y})$, solutions to the inverse problem can be sampled using the score function of these conditional distributions. The most straightforward approach to leverage diffusion models for posterior sampling is to alter the training to accommodate the partial measurements \mathbf{y} [42, 43], modifying Eq. (1) to

$$\mathcal{L} = \mathbb{E} \left[w_t \|m_\theta(\mathbf{x}_t, t, \mathbf{y}) - \mathbf{x}_0\|^2 \right], \quad (5)$$

where $\mathbf{y} = \mathbf{H}\mathbf{x}_0$ for some desired degradation \mathbf{H} . It is common to implement the conditioning on \mathbf{y} by concatenating $\mathbf{H}^\dagger\mathbf{y}$ to the noisy network inputs². $\mathbf{H}^T\mathbf{y}$, or a similar operation that shapes the measurements back into the

² \mathbf{H}^\dagger is the Moore–Penrose pseudo-inverse of the operator \mathbf{H} .

image dimensions can also be used instead. Such methods typically achieve good results, and have proven to be accurate. Yet, such methods are not conditioned on the degradation operator \mathbf{H} , limiting them to a single or few degradations per trained model [42, 43]. Several works extend these frameworks to flow matching [12] and Schrödinger bridges [32]. These methods are beyond the scope of this work, but we expect our architecture to perform equally well for these different training regimes.

An alternative approach is to use an existing unconditional model $m_\theta(\mathbf{x}_t, t)$ and knowledge of \mathbf{H} to model the conditional score $\nabla_{\mathbf{x}_t} \log(p(\mathbf{x}_t|\mathbf{y}, \mathbf{H}))$, using the Bayes rule

$$\begin{aligned} \nabla_{\mathbf{x}_t} \log(p(\mathbf{x}_t|\mathbf{y}, \mathbf{H})) &= \\ & \nabla_{\mathbf{x}_t} \log(p(\mathbf{x}_t)) + \nabla_{\mathbf{x}_t} \log(p(\mathbf{y}|\mathbf{x}_t, \mathbf{H})). \end{aligned} \quad (6)$$

Such methods are referred to as zero-shot [8, 9, 30, 31, 47, 55, 56], for their use of pre-trained diffusion models to solve inverse problem tasks. These methods are highly flexible, for a single trained model can be used to solve any inverse problem for which $\nabla_{\mathbf{x}_t} \log(p(\mathbf{y}|\mathbf{x}_t, \mathbf{H}))$ can be approximated. Yet, these methods are often inaccurate, slow, and computationally expensive, due to the challenge of obtaining an accurate approximation for $\nabla_{\mathbf{x}_t} \log(p(\mathbf{y}|\mathbf{x}_t, \mathbf{H}))$. In contrast to the correctness guarantees of training-based models [4], zero-shot models cannot sample from the posterior even with an ideal denoiser [20].

2.4. Algorithm Unrolling

Algorithm unrolling, also known as deep unfolding or algorithm unrolling, represents a paradigm where iterative algorithms inspired by classical optimization utilize repeated application of neural networks. This approach, first introduced in Gregor and LeCun [19], had emerged into image processing [1, 50, 57]. In inverse problem solving, many algorithm unrolling methods utilize repeated application of \mathbf{H} and \mathbf{H}^\dagger (or \mathbf{H}^T) between network evaluations. Our InverseFusion architecture is inspired by the same principles, but leads to a very different execution. Instead of approximating an iterative algorithm, it treats each of the model’s many layer’s as being unrolled through the degradation. Using the attention mechanism, the model learns where to utilize this additional information.

2.5. Attention for Conditional Generation

Attention mechanisms [53], originally developed for language processing tasks, have emerged as a dominant architectural paradigm in image processing applications. The fundamental operation in attention layers involves matching queries and keys, enabling the network to identify and combine corresponding features across different data streams, and output relevant values. This architectural approach has

found widespread adoption in image generation tasks, particularly in conditional generation scenarios. A prominent example is text-to-image synthesis [41, 43], where cross-attention mechanisms facilitate interaction between textual inputs and internal diffusion model activations. The versatility of attention mechanisms extends beyond text-to-image applications, demonstrating significant utility in various domains, such as image editing [7, 23, 52], novel-view-synthesis [16, 44, 51] and many more.

3. Method

The integration of degradation operators directly as input to neural networks presents significant computational and architectural challenges. The complexity arises from the vast dimensionality of potential degradation representations. Even when considering only linear degradations, each row of the degradation matrix can be as large as the input image itself, creating an overwhelming input space that would render traditional network architectures computationally intractable and practically infeasible.

To address this fundamental challenge, our approach incorporates the degradation operator within the network architecture itself. We introduce a novel *Feature Degradation Layer*, which applies the degradation operator to the internal network activations, and compares the result to the provided measurements, as shown in Fig. 2. Specifically, in this layer, feature representations undergo the following operations: deep features are first rearranged in the shape of a stack or images, to which the degradation is applied. These degraded features are then concatenated with measurements, and are transformed with a learned linear operator, incorporating the information from both the measurements and the degraded features. Finally, the transformed degraded features are mapped back to the feature space through a pseudo-inverse operation. This process can be described formally as

$$\tilde{\mathbf{a}} = \mathbf{H}^\dagger(T_\psi([\mathbf{H}\mathbf{a} \ \mathbf{y}])), \quad (7)$$

where $\mathbf{a} \in \mathbb{R}^{D \times c}$ are the inputs to the layer, and $T_\psi : \mathbb{R}^{(c+1)} \rightarrow \mathbb{R}^c$ is a learned transform and activation operating on the channels axis c .

We interweave the output of our Feature Degradation Layers back into the network’s processing stream using joint-attention, as illustrated in Fig. 2. These complete blocks, which we name *InvFussion Blocks*, are designed to replace standard attention blocks in existing Transformer or UNet architectures. The above operations require that the network’s deep feature resolution match the input image dimension D . This constraint is easy to satisfy in Vision Transformer [11, 15, 39] networks, by simply un-patching the activations back to the original image shape, and using a number of hidden channels that is divisible by the original image channels.

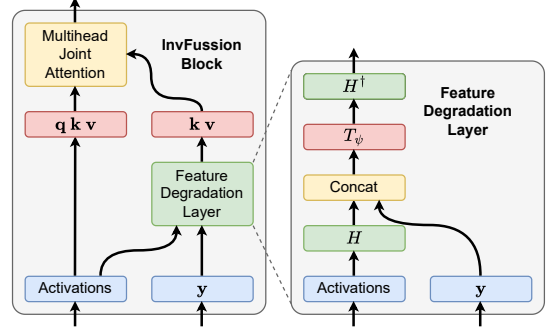


Figure 2. **A diagram of the InvFussion Block.** Our block contains a Feature Degradation Layer, which incorporates the operator \mathbf{H} into the architecture by applying the operator on the activations and comparing them against the measurements $\mathbf{y} = \mathbf{H}\mathbf{x}$.

Finally, using our complete InvFussion architecture, a diffusion model can be trained directly by conditioning on both the degradation and the measurements,

$$\mathcal{L} = \mathbb{E} \left[w_t \|m_\theta(\mathbf{x}_t, t, \mathbf{y}, \mathbf{H}) - \mathbf{x}_0\|^2 \right], \quad (8)$$

where \mathbf{H} is sampled from some pre-determined distribution over possible degradations. Additionally, we also find it is beneficial to concatenate $\mathbf{H}^\dagger \mathbf{y}$ to the noisy network input.

Sampling from InvFussion maintains fundamental compatibility with standard diffusion model sampling procedures, offering a significant advantage in terms of flexibility and implementation. This compatibility means that any established sampling technique developed for conventional diffusion models can be directly applied to InvFussion.

3.1. MMSE Estimator

Our InvFussion architecture can be used for more than posterior sampling. Having an architecture that make use of the degradation \mathbf{H} enables training a single model with

$$\mathcal{L} = \mathbb{E} \left[\|m_\theta(\mathbf{y}, \mathbf{H}) - \mathbf{x}\|^2 \right] \quad (9)$$

to produce MMSE predictors for many different degradations. Alternatively, the MMSE predictor can be approximated by a diffusion model trained with Eq. (8) by applying a single denoising step on white Gaussian noise. That is, for sufficiently small $\alpha(t)$ we have that $\mathbf{x}_t \approx \epsilon$, which is independent of \mathbf{x}_0 , so that

$$\mathbb{E}[\mathbf{x}_0 | \mathbf{x}_t, \mathbf{y}, \mathbf{H}] = \mathbb{E}[\mathbf{x}_0 | \mathbf{y}, \mathbf{H}], \quad (10)$$

which also holds for the approximate models being trained. In other words, any conditional diffusion model can be used as an efficient MMSE predictor. We find that this works well (see App. B), and utilize this in our experiments.



Figure 3. **Examples comparing zero-shot and training-based inverse problem solvers.** For each degradation, the top row is an example from FFHQ64 and the bottom row from ImageNet64. Images generated using training-based methods use deterministic samplers and identical seeds, highlighting the subtle effects the different training algorithms.

4. Experiments

We evaluate the advantage of InvFusion over existing inverse problem solvers on 64×64 images from the FFHQ [27] and ImageNet [13] datasets. In these experiments, we conduct a comparative analysis of InvFusion against alternative methods that can operate on several types of degradations with a single model. This includes zero-shot methods, utilizing an unconditional model which we trained with an equivalent architectural configuration. Additionally, we evaluate our approach against a “Palette”-style methodology [42] that incorporates the $H^{\dagger}y$ as input without additional degradation information. We train this model ourselves using the same underlying architecture, to enable a comprehensive assessment of our method’s capa-

bilities disentangled from architectural considerations. The models trained on ImageNet are also class-conditional, and use CFG [25] with a factor of 2.0 for sampling.

We train and evaluate our model on several categories of inverse problems; strided motion blur (combining various degrees of super-resolution and de-blurring), in-painting by leaving only patches of various sizes, and a general matrix degradation operator. The parameters of each degradation are randomized, to create a large corpus of possible degradations (as detailed in App. A). All conditional models are also trained on unconditional generation by using a degradation which always outputs zeros. Figure 3 shows qualitative comparisons of different inverse problem solving methods for the two datasets. All training-based approaches use the deterministic sampler from EDM [28] along with iden-

Table 1. Comparison of inverse-problem solving methods on FFHQ64. Best method in bold.

Method	Strided Motion Blur			In-Painting			Matrix Operator			NFEs
	PSNR \uparrow	FID \downarrow	C-FID \downarrow	PSNR \uparrow	FID \downarrow	C-FID \downarrow	PSNR \uparrow	FID \downarrow	C-FID \downarrow	
Zero-shot Methods										
DDRM [31]	22.49	23.18	23.16	12.62	53.55	53.55	10.76	72.74	72.74	25
DDNM [55]	23.98	42.52	42.34	16.18	54.59	54.59	11.93	131.37	131.37	100
DPS [9]	18.31	9.66	17.73	10.06	16.96	67.46	9.57	26.86	35.93	1000*
Π GDM [47]	22.12	6.29	6.32	15.20	12.81	12.81	10.71	19.13	19.13	100*
DAPS [56]	17.50	143.45	60.33	16.31	16.91	19.12	11.95	56.30	87.18	1000
Training-based Methods										
Palette [42]	20.97	4.70	5.83	16.97	5.32	5.45	12.50	6.63	25.54	63
InvFussion	22.59	4.65	4.69	17.14	5.08	5.11	14.89	8.33	8.41	63
MMSE estimation methods (Training-based)										
Palette [42]	23.47	-	-	19.65	-	-	15.51	-	-	1
InvFussion	24.74	-	-	19.81	-	-	17.62	-	-	1

Table 2. Comparison of inverse-problem solving methods on ImageNet64. Best method in bold.

Method	Strided Motion Blur			In-Painting			Matrix Operator			NFEs
	PSNR \uparrow	FID \downarrow	C-FID \downarrow	PSNR \uparrow	FID \downarrow	C-FID \downarrow	PSNR \uparrow	FID \downarrow	C-FID \downarrow	
Zero-shot Methods										
DDRM [31]	21.21	26.12	26.22	12.21	30.49	30.49	10.60	32.89	32.89	25
DDNM [55]	22.45	69.47	69.27	15.08	95.27	95.27	11.32	115.32	115.32	100
DPS [9]	18.26	8.96	12.86	10.36	15.23	17.74	9.52	12.80	12.80	1000*
Π GDM [47]	19.99	7.12	7.14	14.29	8.74	8.74	10.59	8.93	8.93	100*
DAPS [56]	17.32	125.73	62.81	15.35	16.31	19.66	11.65	28.27	37.03	1000
Training-based Methods										
Palette [42]	19.61	6.60	6.97	15.56	6.20	6.20	12.34	6.70	11.44	63
InvFussion	20.80	6.21	6.21	15.58	6.44	6.44	14.38	6.87	6.87	63
MMSE estimation methods (Training-based)										
Palette [42]	22.25	-	-	18.32	-	-	15.28	-	-	1
InvFussion	23.19	-	-	18.34	-	-	17.12	-	-	1

* Methods that use the derivative of the network, leading to more computation and memory per NFE.

tical seeds, highlighting the effects of different models.

For quantitative comparisons, we use PSNR to measure the image fidelity, *i.e.* how close the restored output is to the original. To measure image realism, we use 10K FID [24]. These two metrics are at odds according to the Perception-Distortion-Tradeoff [6], and different methods excel at either of the metrics. We also find that some restoration algorithms sacrifice consistency with the measurements \mathbf{y} to accommodate better image realism, in effect ignoring the inverse problem. To measure the image realism of valid solutions to the given inverse problem, we offer to measure the FID of generated samples that have been projected to

be consistent with the measurements \mathbf{y} , which we refer to as C-FID. In this way, we penalize models for the distance between the generated sample and the nearest valid solution to the formulated problem. Tables 1 and 2 show our qualitative analysis on the FFHQ [27] and ImageNet [13] datasets respectively. Our model achieves the best C-FID among all training-based and zero-shot methods in all but a single case, suggesting it is SOTA in generating samples from the posterior. Our InvFussion MMSE estimator based on the same model achieves the best PSNR of all models, while the InvFussion posterior sampler is also among the highest in PSNR. This is also reflected in the qualitative examples

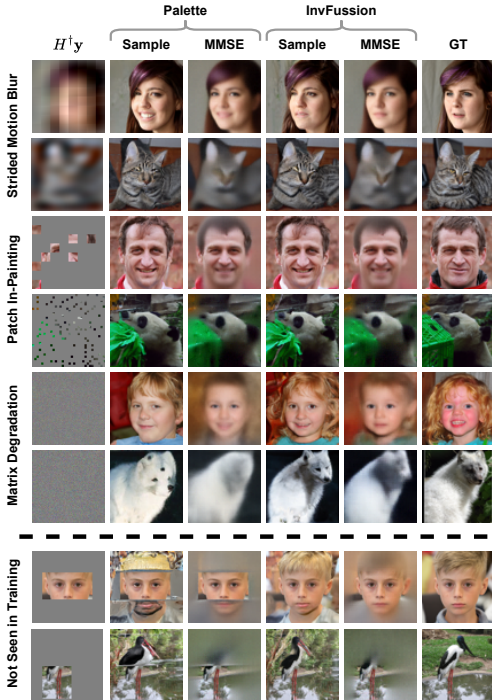


Figure 4. Examples comparing MMSE estimators and samples from the posterior for InvFussion against a baseline that is not degradation-aware. InvFussion model is equivalent or superior in both posterior sampling and MMSE estimation.

for MMSE estimation in Fig. 4.

Interestingly, the gap in performance between InvFussion and Palette highly varies between different degradation families. In problems like in-painting, the degradation is easily inferrable by the network, as the $H^t y$ input to the network contains masked regions (see Fig. 3). Thus in in-painting, we see marginal to no advantage for InvFussion over Palette. On the other hand, in motion-blur and even more so on general matrix degradations, the Palette model struggles to infer the exact degradation, leading to a drop in both PSNR and C-FID, sometimes, even lower than some zero-shot methods which are degradation-aware. This supports our hypothesis that knowledge of the degradation operator, whether inferred or explicit, is critical for correct restoration.

To demonstrate InvFussion’s scalability and performance at higher resolutions, we conducted additional experiments using 256×256 images from FFHQ. The complete results are presented in App. C, with representative examples shown in Fig. 1.

4.1. Out-Of-Distribution Degradations and Unconditional Sampling

To measure the generalization capabilities of different methods we evaluate performance on a degradation that is

Table 3. Comparison of restoration on a degradation that did not appear in training. InvFussion demonstrates strong adaptation capabilities through its degradation-aware architecture.

Method	PSNR \uparrow	FID \downarrow	C-FID \downarrow
Zero-shot Methods			
DDRM [31]	11.59	24.85	24.85
DDNM [55]	12.69	75.81	75.81
DPS [9]	10.09	8.78	14.10
PIGDM [47]	11.28	7.26	7.26
DAPS [56]	12.12	40.84	39.53
Training-based Methods			
Palette [42]	10.97	19.91	19.89
InvFussion	11.85	5.73	5.73
MSE estimation methods (Training-based)			
Palette [42]	13.58	-	-
InvFussion	14.71	-	-

Table 4. Comparison of unconditional sampling.

Method	FFHQ FID \downarrow	ImageNet FID \downarrow
Baseline [11]	6.66	8.98
Palette [42]	6.56	8.26
InvFussion	6.27	8.19

slightly outside of the training distribution. In this case, we perform out-painting from a single rectangular area in the image. The results in Tab. 3, show that Palette completely fails to generalize, despite the similarity to the in-painting task the model has been trained on and the ease at which the degradation operator can be inferred from the input. On the other hand, InvFussion does quite well on this problem, outperforming all zero-shot methods, which are not penalized by the out-of-distribution (OOD) degradation, as they are not trained on any degradation. Finally, we also evaluate all trained models for unconditional generation (on which they had been trained, by using $H \in R^{0 \times D}$). Surprisingly, we find that both inverse-problem models outperform the unconditional baseline, with InvFussion leading with a 7% improvement over the baseline (unconditional diffusion). This is despite the conditional models having no additional capacity, as both the additional model inputs and the Feature Degradation Layer are always output zeros for unconditional sampling. We hypothesize that being exposed to partial image information during training helps the diffusion model converge faster.

4.2. Noisy Degradations

Following the noiseless linear case explored in 4, we also conduct experiments on noisy inverse problems. We retrain the FFHQ64 model, incorporating additive white Gaussian noise with a standard deviation of $\sigma_n = 0.1$ in the measurements \mathbf{y} . The InvFusion architecture remains unchanged, using only the transforms \mathbf{H} and \mathbf{H}^\dagger of the degradation – as adding randomly sampled noise at each layer could lead to accumulation of noise. Projection operators are not well-defined for noisy degradations, so only PSNR and FID are evaluated for the noisy case. Our findings in Tab. 8 (App. C) demonstrate the advantage of InvFusion over alternative methods in the noisy settings.

5. Neural Posterior Principal Components

Beyond the improvements in restoration fidelity and realism, using an operator-aware architecture unlocks several capabilities that are useful for down stream applications. A notable example, is the computation of Neural Posterior Principal Components (NPPCs) [38], which are efficient estimations of the posterior distribution’s largest principal vectors. These direction are meaningful for uncertainty quantification among many other tasks [18, 36], and may have high implications for medical analysis [5, 17]. In the original work by Nehme et al. [38], a network is trained to approximate the posterior principal components for a single pre-defined degradation. Using InvFusion, we can use the same approach to scale up NPPC training to multiple degradations at once, enabling flexible adaptation to the degradation at runtime. We experiment with applying the exact same NPPC loss from [38], using the InvFusion architecture to condition the network on the degradation operator \mathbf{H} for the in-painting of a single area of the image. The examples in Figure 5 shows that InvFusion meaningfully extends NPPC computation for multiple degradation, making a single model viable for a wide range of problems.

6. Discussion, Limitations and Conclusion

Despite achieving state-of-the-art performance in posterior sampling and MMSE estimation, InvFusion faces several important limitations. A primary constraint lies in the model’s training scope – although InvFusion demonstrates remarkable adaptability to various degradations, it can only be trained on a finite set of degradation types. Even in the linear case, the space of possible degradations scales quadratically with image dimensions, creating fundamental constraints that would be impractical to address solely through increased model capacity and training time. Additionally, while our current results focus exclusively on linear degradations, we anticipate that InvFusion could potentially generalize to non-linear degradations when appropriately trained, though this remains to be empirically vali-

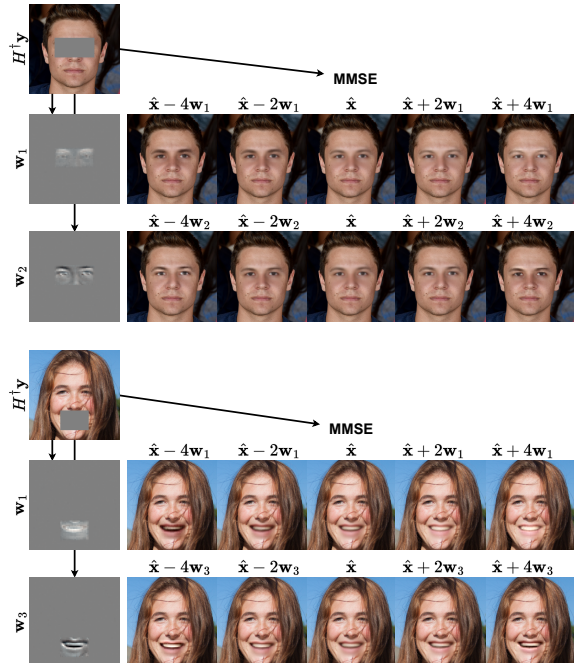


Figure 5. **Examples of Using InvFusion for NPPC.** By being degradation-aware, the model can be trained to predict the MMSE and several leading principle components \mathbf{w}_i (shown on the left, contrast enhanced) for many degradations.

dated. A final consideration is the computational and memory intensity of repeated degradation applications, particularly during the training phase. Although this computational overhead may be relatively minor compared to certain zero-shot methods that require additional steps or model derivatives, optimizing these resource requirements represents a key area for future improvement.

This work introduces InvFusion, a novel architectural framework that bridges the long-standing gap between training-based and zero-shot approaches in solving inverse problems with diffusion models. By incorporating the degradation operator directly into the network architecture through attention-based layer unrolling, our method achieves state-of-the-art performance while maintaining the flexibility to handle diverse degradation scenarios. The empirical results demonstrate superior performance on multiple dataset across various inverse problems, while offering computational efficiency comparable to existing methods. Beyond its primary application, InvFusion’s capability as a general MMSE estimator and its potential for NPPC estimation opens new avenues for downstream applications. While certain limitations remain, this work represents a significant step forward in the field of accurate and efficient inverse problem solving.

Acknowledgments

This research was partially supported by the Israel Science Foundation (ISF) under Grants 2318/22, 951/24 and 409/24, and by the Council for Higher Education – Planning and Budgeting Committee.

References

- [1] Hemant K Aggarwal, Merry P Mani, and Mathews Jacob. Modl: Model-based deep learning architecture for inverse problems. *IEEE transactions on medical imaging*, 38(2): 394–405, 2018. [2](#), [3](#)
- [2] Guillaume Alain and Yoshua Bengio. What regularized auto-encoders learn from the data-generating distribution. *The Journal of Machine Learning Research*, 15(1):3563–3593, 2014. [2](#)
- [3] Brian DO Anderson. Reverse-time diffusion equation models. *Stochastic Processes and their Applications*, 12(3):313–326, 1982. [2](#)
- [4] Georgios Batzolis, Jan Stanczuk, Carola-Bibiane Schönlieb, and Christian Etmann. Conditional image generation with score-based diffusion models. *arXiv preprint arXiv:2111.13606*, 2021. [3](#)
- [5] Omer Belhasin, Yaniv Romano, Daniel Freedman, Ehud Rivlin, and Michael Elad. Principal uncertainty quantification with spatial correlation for image restoration problems. *IEEE Transactions on Pattern Analysis and Machine Intelligence*, 2023. [8](#)
- [6] Yochai Blau and Tomer Michaeli. The perception-distortion tradeoff. In *Proceedings of the IEEE conference on computer vision and pattern recognition*, pages 6228–6237, 2018. [6](#)
- [7] Mingdeng Cao, Xintao Wang, Zhongang Qi, Ying Shan, Xiaohu Qie, and Yinqiang Zheng. Masactrl: Tuning-free mutual self-attention control for consistent image synthesis and editing. In *Proceedings of the IEEE/CVF International Conference on Computer Vision (ICCV)*, pages 22560–22570, 2023. [4](#)
- [8] Hyungjin Chung, Byeongsu Sim, Dohoon Ryu, and Jong Chul Ye. Improving diffusion models for inverse problems using manifold constraints. *Advances in Neural Information Processing Systems*, 35:25683–25696, 2022. [1](#), [3](#)
- [9] Hyungjin Chung, Jeongsol Kim, Michael Thompson McCann, Marc Louis Klasky, and Jong Chul Ye. Diffusion posterior sampling for general noisy inverse problems. In *The Eleventh International Conference on Learning Representations*, 2023. [1](#), [3](#), [6](#), [7](#), [13](#), [14](#), [15](#)
- [10] Hyungjin Chung, Jeongsol Kim, Geon Yeong Park, Hyelin Nam, and Jong Chul Ye. Cfg++: Manifold-constrained classifier free guidance for diffusion models. *arXiv preprint arXiv:2406.08070*, 2024. [2](#)
- [11] Katherine Crowson, Stefan Andreas Baumann, Alex Birch, Tanishq Mathew Abraham, Daniel Z Kaplan, and Enrico Shippole. Scalable high-resolution pixel-space image synthesis with hourglass diffusion transformers. In *Forty-first International Conference on Machine Learning*, 2024. [2](#), [4](#), [7](#), [12](#)
- [12] Mauricio Delbracio and Peyman Milanfar. Inversion by direct iteration: An alternative to denoising diffusion for image restoration. *arXiv preprint arXiv:2303.11435*, 2023. [3](#)
- [13] Jia Deng, Wei Dong, Richard Socher, Li-Jia Li, Kai Li, and Li Fei-Fei. ImageNet: A large-scale hierarchical image database. In *2009 IEEE Conference on Computer Vision and Pattern Recognition*, pages 248–255, 2009. [2](#), [5](#), [6](#)
- [14] Prafulla Dhariwal and Alexander Nichol. Diffusion models beat GANs on image synthesis. *Advances in Neural Information Processing Systems*, 34:8780–8794, 2021. [1](#)
- [15] Alexey Dosovitskiy, Lucas Beyer, Alexander Kolesnikov, Dirk Weissenborn, Xiaohua Zhai, Thomas Unterthiner, Mostafa Dehghani, Matthias Minderer, Georg Heigold, Sylvain Gelly, Jakob Uszkoreit, and Neil Houlsby. An image is worth 16x16 words: Transformers for image recognition at scale, 2021. [2](#), [4](#)
- [16] Noam Elata, Bahjat Kawar, Yaron Ostrovsky-Berman, Miriam Farber, and Ron Sokolovsky. Novel view synthesis with pixel-space diffusion models. *arXiv preprint arXiv:2411.07765*, 2024. [4](#)
- [17] Noam Elata, Tomer Michaeli, and Michael Elad. Adaptive compressed sensing with diffusion-based posterior sampling. In *European Conference on Computer Vision*, pages 290–308. Springer, 2025. [8](#)
- [18] Noam Elata, Tomer Michaeli, and Michael Elad. Psc: Posterior sampling-based compression, 2025. [8](#)
- [19] Karol Gregor and Yann LeCun. Learning fast approximations of sparse coding. In *Proceedings of the 27th international conference on machine learning*, pages 399–406, 2010. [3](#)
- [20] Shivam Gupta, Ajil Jalal, Aditya Parulekar, Eric Price, and Zhiyang Xun. Diffusion posterior sampling is computationally intractable. *arXiv preprint arXiv:2402.12727*, 2024. [3](#)
- [21] Ali Hassani, Steven Walton, Jiachen Li, Shen Li, and Humphrey Shi. Neighborhood attention transformer. In *IEEE/CVF Conference on Computer Vision and Pattern Recognition (CVPR)*, 2023. [12](#)
- [22] Ali Hassani, Wen-Mei Hwu, and Humphrey Shi. Faster neighborhood attention: Reducing the $O(n^2)$ cost of self attention at the threadblock level. In *Advances in Neural Information Processing Systems*, 2024. [12](#)
- [23] Amir Hertz, Ron Mokady, Jay Tenenbaum, Kfir Aberman, Yael Pritch, and Daniel Cohen-Or. Prompt-to-prompt image editing with cross attention control. *arXiv preprint arXiv:2208.01626*, 2022. [4](#)
- [24] Martin Heusel, Hubert Ramsauer, Thomas Unterthiner, Bernhard Nessler, and Sepp Hochreiter. Gans trained by a two time-scale update rule converge to a local nash equilibrium. In *Advances in Neural Information Processing Systems*, 2017. [6](#)
- [25] Jonathan Ho and Tim Salimans. Classifier-free diffusion guidance. *arXiv preprint arXiv:2207.12598*, 2022. [2](#), [5](#), [14](#)
- [26] Jonathan Ho, Ajay Jain, and Pieter Abbeel. Denoising diffusion probabilistic models. *Advances in Neural Information Processing Systems*, 33:6840–6851, 2020. [1](#), [2](#)
- [27] Tero Karras. A style-based generator architecture for generative adversarial networks. *arXiv preprint arXiv:1812.04948*, 2019. [2](#), [5](#), [6](#)

- [28] Tero Karras, Miika Aittala, Timo Aila, and Samuli Laine. Elucidating the design space of diffusion-based generative models. *Advances in neural information processing systems*, 35:26565–26577, 2022. 2, 5, 12
- [29] Tero Karras, Miika Aittala, Jaakko Lehtinen, Janne Hellsten, Timo Aila, and Samuli Laine. Analyzing and improving the training dynamics of diffusion models. *arXiv preprint arXiv:2312.02696*, 2023. 12
- [30] Bahjat Kawar, Gregory Vaksman, and Michael Elad. Snips: Solving noisy inverse problems stochastically. *Advances in Neural Information Processing Systems*, 34:21757–21769, 2021. 1, 3
- [31] Bahjat Kawar, Michael Elad, Stefano Ermon, and Jiaming Song. Denoising diffusion restoration models. In *Advances in Neural Information Processing Systems*, 2022. 1, 3, 6, 7, 13, 14, 15
- [32] Guan-Hong Liu, Arash Vahdat, De-An Huang, Evangelos A Theodorou, Weili Nie, and Anima Anandkumar. I2sb: image-to-image schrödinger bridge. In *Proceedings of the 40th International Conference on Machine Learning*, pages 22042–22062, 2023. 3
- [33] Cheng Lu, Yuhao Zhou, Fan Bao, Jianfei Chen, Chongxuan Li, and Jun Zhu. Dpm-solver: A fast ode solver for diffusion probabilistic model sampling in around 10 steps. *arXiv preprint arXiv:2206.00927*, 2022. 2
- [34] Cheng Lu, Yuhao Zhou, Fan Bao, Jianfei Chen, Chongxuan Li, and Jun Zhu. Dpm-solver++: Fast solver for guided sampling of diffusion probabilistic models. *arXiv preprint arXiv:2211.01095*, 2022. 2
- [35] Andreas Lugmayr, Martin Danelljan, Andres Romero, Fisher Yu, Radu Timofte, and Luc Van Gool. Repaint: Inpainting using denoising diffusion probabilistic models. In *Proceedings of the IEEE/CVF conference on computer vision and pattern recognition*, pages 11461–11471, 2022. 1
- [36] Hila Manor and Tomer Michaeli. On the posterior distribution in denoising: Application to uncertainty quantification. *arXiv preprint arXiv:2309.13598*, 2023. 8
- [37] Dimitra Maoutsa, Sebastian Reich, and Manfred Opper. Interacting particle solutions of fokker–planck equations through gradient–log–density estimation. *Entropy*, 22(8): 802, 2020. 2
- [38] Elias Nehme, Omer Yair, and Tomer Michaeli. Uncertainty quantification via neural posterior principal components. *Advances in Neural Information Processing Systems*, 36, 2024. 2, 8
- [39] William Peebles and Saining Xie. Scalable diffusion models with transformers. *arXiv preprint arXiv:2212.09748*, 2022. 2, 4
- [40] Robin Rombach, Andreas Blattmann, Dominik Lorenz, Patrick Esser, and Björn Ommer. High-resolution image synthesis with latent diffusion models. In *Proceedings of the IEEE/CVF Conference on Computer Vision and Pattern Recognition (CVPR)*, pages 10684–10695, 2022. 1
- [41] Robin Rombach, Andreas Blattmann, Dominik Lorenz, Patrick Esser, and Björn Ommer. High-resolution image synthesis with latent diffusion models. In *Proceedings of the IEEE/CVF conference on computer vision and pattern recognition*, pages 10684–10695, 2022. 4
- [42] Chitwan Saharia, William Chan, Huiwen Chang, Chris Lee, Jonathan Ho, Tim Salimans, David Fleet, and Mohammad Norouzi. Palette: Image-to-image diffusion models. In *ACM SIGGRAPH 2022 conference proceedings*, pages 1–10, 2022. 1, 3, 5, 6, 7, 14, 15
- [43] Chitwan Saharia, Jonathan Ho, William Chan, Tim Salimans, David J Fleet, and Mohammad Norouzi. Image super-resolution via iterative refinement. *IEEE transactions on pattern analysis and machine intelligence*, 45(4):4713–4726, 2022. 1, 3, 4
- [44] Junyoung Seo, Kazumi Fukuda, Takashi Shibuya, Takuya Narihira, Naoki Murata, Shoukang Hu, Chieh-Hsin Lai, Seungryong Kim, and Yuki Mitsufuji. Genwarp: Single image to novel views with semantic-preserving generative warping. *arXiv preprint arXiv:2405.17251*, 2024. 4
- [45] Jascha Sohl-Dickstein, Eric Weiss, Niru Maheswaranathan, and Surya Ganguli. Deep unsupervised learning using nonequilibrium thermodynamics. In *International Conference on Machine Learning*, pages 2256–2265. PMLR, 2015. 1, 2
- [46] Jiaming Song, Chenlin Meng, and Stefano Ermon. Denoising diffusion implicit models. In *International Conference on Learning Representations*, 2020. 2
- [47] Jiaming Song, Arash Vahdat, Morteza Mardani, and Jan Kautz. Pseudoinverse-guided diffusion models for inverse problems. In *International Conference on Learning Representations*, 2023. 1, 3, 6, 7, 13, 14, 15
- [48] Yang Song and Stefano Ermon. Generative modeling by estimating gradients of the data distribution. *Advances in Neural Information Processing Systems*, 32, 2019. 1, 2
- [49] Yang Song, Jascha Sohl-Dickstein, Diederik P Kingma, Abhishek Kumar, Stefano Ermon, and Ben Poole. Score-based generative modeling through stochastic differential equations. In *International Conference on Learning Representations*, 2020. 2
- [50] Jian Sun, Huibin Li, Zongben Xu, et al. Deep admn-net for compressive sensing mri. *Advances in neural information processing systems*, 29, 2016. 2, 3
- [51] Hung-Yu Tseng, Qinbo Li, Changil Kim, Suhub Alsisan, Jia-Bin Huang, and Johannes Kopf. Consistent view synthesis with pose-guided diffusion models. In *Proceedings of the IEEE/CVF Conference on Computer Vision and Pattern Recognition*, pages 16773–16783, 2023. 4
- [52] Narek Tumanyan, Michal Geyer, Shai Bagon, and Tali Dekel. Plug-and-play diffusion features for text-driven image-to-image translation. In *Proceedings of the IEEE/CVF Conference on Computer Vision and Pattern Recognition (CVPR)*, pages 1921–1930, 2023. 4
- [53] Ashish Vaswani, Noam Shazeer, Niki Parmar, Jakob Uszkoreit, Llion Jones, Aidan N Gomez, Łukasz Kaiser, and Illia Polosukhin. Attention is all you need. In *Advances in Neural Information Processing Systems*. Curran Associates, Inc., 2017. 2, 3
- [54] Pascal Vincent. A connection between score matching and denoising autoencoders. *Neural computation*, 23(7):1661–1674, 2011. 2
- [55] Yinhuai Wang, Jiwen Yu, and Jian Zhang. Zero-shot image restoration using denoising diffusion null-space model. *The*

Eleventh International Conference on Learning Representations, 2023. [3](#), [6](#), [7](#), [13](#), [14](#), [15](#)

- [56] Bingliang Zhang, Wenda Chu, Julius Berner, Chenlin Meng, Anima Anandkumar, and Yang Song. Improving diffusion inverse problem solving with decoupled noise annealing, 2024. [3](#), [6](#), [7](#), [13](#), [14](#), [15](#)
- [57] Jian Zhang and Bernard Ghanem. Ista-net: Interpretable optimization-inspired deep network for image compressive sensing. In *Proceedings of the IEEE conference on computer vision and pattern recognition*, pages 1828–1837, 2018. [2](#), [3](#)

A. Implementation Details

A.1. Architecture and Model Training

We plan to publish our code implementation and model checkpoints upon acceptance.

We implement all models using the official implementation of HDiT [11] ImageTransformerDenoiserModelV2 architecture. We use default hyperparameters, with changes listed in Tab. 5. The initial patch size is indicated in the graph, with the patch size doubling with the progression along the list shown in the ‘Depths’ column. The attention type column signified which type of attention was used. ‘NAtten x ’ indicates neighborhood attention [21, 22] with a kernel of size x , which preforms attention between patches only in an x sized neighborhood. ‘GAtten’ indicates global attention. As described in Sec. 3, InvFussion requires that all layer widths are divisible by the input channels, which in this case is 3. Also each layer’s width times the layer’s feature map resolution must be a multiple of the input dimension D . In our experiments, this held for all but the deepest layers in the FFHQ256 model. For this reason, we did not apply InvFussion to these layers, and used the baseline unconditional attention implementation instead. This provides evidence that our InvFussion architecture works even when not applied evenly on all the network’s attention layers. In preliminary experiments, we found joint-attention, in which keys and values from the feature degradation layer are concatenated with the keys and value in the main (self) stream, is preferable to applying self-attention followed by cross-attention.

Models are trained and evaluated with the official implementation of the EDM2 [29] training script, using the default $P_{\text{mean}} = -0.8$, $P_{\text{std}} = 1.6$, float16 mixed precision, and a learning rate of $5e - 5$, using the default learning rate scheduler. Sampling is done with the default Heun scheduler using a total of NFEs for sampling. Additional experiment specific-training hyperparameters can be found in Tab. 6. The augmentation implementation and hyperparameters are cloned from EDM [28].

A.2. Degradations

Below we explain the implementation details of each family of degradations used in the paper. Several of the degradations include some form of zero-padding to rows of the degradations H (in its matrix form) and therefore to the measurements y for practical reasons. This is done such that different degradations can be applied in batched form. This produces identical results, as the linear transform T_{ψ} operates on the channel dimension only, and H^{\dagger} would similarly have zero-padded columns.

A.2.1. Patch In-Painting

Patch in-painting is implemented as any in-painting mask where $p \in (0, 0.1)$ of patches of some unvarying size are

visible. When creating a new mask, the patch size, p , and visible patches are randomly sampled until a valid mask in which some patches are visible is created. We preform this “rejection sampling” to remove masks in which no patches are visible.

The pseudo-inverse of a masking operator is itself, thus the computation of H^{\dagger} is trivial. In practice, we retain zeros in the masked measurements y , which is equivalent computationally, to enable different masks with different number of masked pixels across the batch dimension.

A.2.2. Strided Motion-Blur

This family of degradations implements a strided convolution operator, for which we specifically choose a motion-blur kernel. To create a new degradation operator, we first sample a motion-blur kernel the size of the input image using the motionblur library³. We then sample a stride size from [2, 4, 8] and smooth the motion-blur kernel by convolving it with a isometric Gaussian kernel with standard deviation equal to the stride. The kernels are normalized for numeric stability.

The strided convolution is applied in the frequency space for efficient computation, as this is more efficient for large convolution kernels and simplifies the computation and application of the pseudo-inverse operator. At runtime, the given image or activations are transform to the Fourier domain, where they are multiplied with the pre-computed frequency-space operator.

A.2.3. Matrix Degradation

The matrix degradation is a matrix operator with (1, 128) rows, each of which is sampled from a multivariate normal distribution and normalized. The number of rows is limited to enable the use of different matrices across the batch dimension, which is more computationally intensive. The pseudo-inverse operator is computed directly with pytorch’s `p_inv` function.

As any degradation can be represented by a matrix, this family represents all possible degradations in theory. Yet, we find that a model trained only on randomly sampled matrices as described here does not generalize well to specific tasks such as in-painting, super-resolution, or de-blurring.

A.2.4. Box Out-Painting

This degradation is similar to the patch in-painting, but instead of masking all but several patches the box out-painting leaves only a single rectangle of the image visible. To create this degradation we uniformly sample two different coordinates in the image and mask all pixels outside the rectangle that is formed. The practical implementation details are identical to the patch in-painting degradation.

³<https://github.com/LeviBorodenko/motionblur>

Table 5. Architecture Hyperparams

Experiment	Patch Size	Depths	Widths	Attention Type
FFHQ64	(2, 2)	[2, 2, 8]	[384, 768, 1536]	[NAtten7, NAtten7, GAtten]
ImageNet64	(2, 2)	[2, 2, 8]	[384, 768, 1536]	[NAtten7, NAtten7, GAtten]
FFHQ256	(4, 4)	[2, 2, 4, 2]	[192, 384, 768, 1536]	[NAtten5, NAtten7, GAtten, GAtten]

Table 6. Training Hyperparams

Experiment	Iters	Batch	Aug Prob	Label Dropout
FFHQ64	2^{16}	512	0.12	-
ImageNet64	2^{18}	512	0.0	0.1
FFHQ256	2^{18}	256	0.12	-

A.3. Zero-Shot Methods

We use our own implementations for all zero-shot methods, using the default hyperparameter unless specified otherwise. We use the variance-exploding notation, and we adjust all sampling algorithms accordingly. DPS [9] and DAPS [56] only require access to the degradation operator H , while DDNM [55] and Π GDM [47] also make use of the pseudo-inverse operator H^\dagger . In the original implementation DDRM [31] makes use of the complete SVD of the operator H . Because obtaining this SVD is computationally expensive (or even practically impossible in reasonable time) for most of our degradations, we instead implement the DDRM algorithm using only H and H^\dagger . For the noiseless case, this implementation is equivalent to the original implementation. This is not true case in the general noisy case, unless all the degradation’s singular values that are not zeros are equal. Due to the degradation families we choose to apply, we assume that most of the singular values that are not zeros are nearly one for the purpose of implementing DDRM in the noisy degradation experiment. For Π GDM, we make a similar assumption to implement the noisy sampling algorithm, to avoid inverting a large matrix. For the in-painting case, the assumption holds. Similarly, in the strided motion-blur we make use of the fact that white Gaussian noise remains white Gaussian noise under a Fourier transform, and that the application of the kernel is multiplicative.

B. Using Diffusion Models for MMSE

In Sec. 3.1 we explore the use of the InvFussion architecture of MMSE estimation. A DNN can be trained directly as a degradation-aware MMSE estimator using a regression loss as seen in Eq. (9). Nevertheless, we notice that we can utilize our existing trained diffusion models (trained using Eq. (8)) for the same task. Intuitively, this is because for sufficiently high noise values, the noisy input to the network is

equivalent to pure noise. Therefore, The network learns to rely only on the information from y and H . In practice, we use the value $\sigma_t = 100$ for the MMSE estimation.

We test the gap between models trained directly for MMSE estimation (Eq. (9)) and models trained for diffusion (Eq. (8)) on FFHQ64, using the same architecture. The MMSE model’s input is Gaussian noise, instead of the noisy image input to the diffusion model, to keep the architecture identical. The results in Tab. 7 reflect that both methods yield approximately the same results, whether trained using the degradation-aware InvFussion architecture and loss or without it. We conclude that it is probably more cost-effective to use a single model for both posterior sampling and MMSE estimation task, and do so for the experiments in our paper.

C. Additional Results

C.1. Noisy Degradations

Table 8 shows the results of the experiment described in Sec. 4.2. The results show that InvFussion maintains superiority when noise is added to the degradation. We expect this framework to work well across many noise types, not limited to white Gaussian noise, as the model learns to treat the noise through training, which does not rely on any fundamental properties of the noise.

C.2. FFHQ 256

Table 9 shows quantitative results for our experiment on 256×256 FFHQ images. InvFussion remains the SOTA method as measured by C-FID – the perceptual image quality of valid solutions to the inverse problem.

C.3. Unconditional Samples

Figures 6 and 7 show qualitative examples for unconditional samples from our model *i.e.* samples that are not conditioned on a measurement vector y . The models trained

Table 7. Comparison of MMSE training and diffusion models used for MMSE.

Architecture & Loss	Strided Motion Blur	In-Painting	Matrix Operator
	PSNR \uparrow	PSNR \uparrow	PSNR \uparrow
Trained for MMSE (Eq. (9))			
Palette [42]	23.08	19.36	15.63
InvFussion	24.66	19.79	17.92
Trained For diffusion (Eq. (8))			
Palette [42]	23.47	19.65	15.51
InvFussion	24.74	19.81	17.62

Table 8. Comparison of noisy inverse-problem solving methods on FFHQ64.

Method	Strided Motion Blur		In-Painting		Matrix Operator		NFEs
	PSNR \uparrow	FID \downarrow	PSNR \uparrow	FID \downarrow	PSNR \uparrow	FID \downarrow	
Zero-shot Methods							
DDRM [31]	11.69	137.04	12.21	155.59	11.80	86.72	25
DDNM [55]	19.82	97.22	17.26	46.44	11.94	96.52	100
DPS [9]	6.98	12.34	8.26	7.77	9.18	27.33	1000*
Π IGDM [47]	16.49	11.50	15.69	21.56	10.76	10.91	100*
DAPS [56]	16.90	46.41	15.54	43.72	10.57	58.67	1000
Training-based Methods							
Palette [42]	17.09	6.05	16.70	5.21	12.58	6.59	63
InvFussion	18.09	5.39	16.81	4.57	14.70	6.51	63
MMSE estimation methods (Training-based)							
Palette [42]	19.82	-	18.89	-	15.59	-	1
InvFussion	20.67	-	19.61	-	17.48	-	1

on ImageNet are conditioned on the class label, and use CFG [25] coefficient of 2.0 to enhance the image quality.

Table 9. Comparison of inverse-problem solving methods on FFHQ256.

Method	Strided Motion Blur			In-Painting			NFEs
	PSNR \uparrow	FID \downarrow	C-FID \downarrow	PSNR \uparrow	FID \downarrow	C-FID \downarrow	
Zero-shot Methods							
DDRM [31]	25.33	45.21	45.22	12.76	103.96	103.96	25
DDNM [55]	26.21	51.19	51.15	14.25	105.51	105.51	100
DPS [9]	22.70	18.32	22.42	9.71	26.67	94.34	1000*
Π GDM [47]	24.63	11.81	11.82	16.66	26.63	26.63	100*
DAPS [56]	15.11	286.76	96.40	16.99	44.96	50.59	1000
Training-based Methods							
Palette [42]	23.20	8.67	11.86	18.22	10.65	11.89	63
InvFussion	23.75	9.52	10.70	18.54	10.64	10.78	63



Figure 6. Examples of unconditional samples from FFHQ.

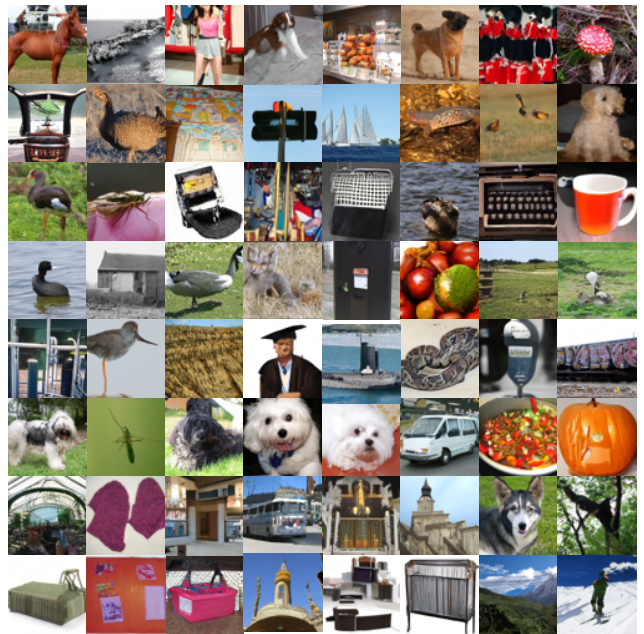


Figure 7. Examples of class-conditional samples from ImageNet. Samples are not conditioned on any measurements y , and are sampled with CFG of 2.0 on the class conditioning.